POLITECNICO DI TORINO
Repository ISTITUZIONALE

Test-Driven Design of an Active Dual-Polarized Log-Periodic Antenna for the Square Kilometre Array

Original
Test-Driven Design of an Active Dual-Polarized Log-Periodic Antenna for the Square Kilometre Array / Bolli, P., Mezzadrelli, L., Monari, J., Perini, F., Tibaldi, A., Virone, G., Bercigli, M., Ciorba, L., Paonessa, F., Rusticelli, S., Schiaffino, M.. - In: IEEE OPEN JOURNAL OF ANTENNAS AND PROPAGATION. - ISSN 2637-6431. - ELETTRONICO. - 1:(2020), pp. 253-263. [10.1109/OJAP.2020.2999109]

Availability:
This version is available at: 11583/2836622 since: 2020-06-19T06:33:45Z

Publisher:
IEEE

Published
DOI:10.1109/OJAP.2020.2999109

Terms of use:

This article is made available under terms and conditions as specified in the corresponding bibliographic description in the repository

Publisher copyright
IEEE postprint/Author's Accepted Manuscript

©2020 IEEE. Personal use of this material is permitted. Permission from IEEE must be obtained for all other uses, in any current or future media, including reprinting/republishing this material for advertising or promotional purposes, creating new collecting works, for resale or lists, or reuse of any copyrighted component of this work in other works.

(Article begins on next page)

14 November 2026

Received 24 April 2020; revised 23 May 2020; accepted 25 May 2020. Date of publication 3 June 2020; date of current version 17 June 2020.

Digital Object Identifier 10.1109/OJAP.2020.2999109

Test-Driven Design of an Active Dual-Polarized Log-Periodic Antenna for the Square Kilometre Array

PIETRO BOLLI[1], LORENZO MEZZADRELLI[2], JADER MONARI[3], FEDERICO PERINI[3], ALBERTO TIBALDI[4,5] (Member, IEEE), GIUSEPPE VIRONE[5] (Member, IEEE), MIRKO BERCIGLI[6], LORENZO CIORBA[4,5], PAOLA DI NINNI[1], MARIA GRAZIA LABATE[7], VITTORIO GIUSEPPE LOI[2], ANDREA MATTANA[3], FABIO PAONESSA[5] (Member, IEEE), SIMONE RUSTICELLI[3], AND MARCO SCHIAFFINO[3]

[1]Astrophysical Observatory of Florence, INAF, 50125 Florence, Italy

[2]Department of Research and Development, Sirio Antenne, 46049 Volta Mantovana, Italy

[3]Institute of Radioastronomy, INAF, 40129 Bologna, Italy

[4]Department of Electronics and Telecommunications, Politecnico di Torino, 10129 Turin, Italy

[5]Institute of Electronics, Computer and Telecommunication Engineering, CNR, 10129 Turin, Italy

[6]Department of Computational Electromagnetic Engineering, Ingegneria dei Sistemi, 56121 Pisa, Italy

[7]Department of Project Engineering, Square Kilometre Array Organization, Lower Withington SK11 9FT, U.K.

CORRESPONDING AUTHOR: P. BOLLI (e-mail: pbolli@arcetri.inaf.it)

ABSTRACT An active dual-polarized Log-Periodic antenna has been designed to meet the requirements of the low-frequency (50 - 350 MHz) radio telescope of the Square Kilometre Array (SKA). The integration of antenna and low noise amplifier has been conceived in order to achieve a high degree of testability. This aspect has been found to be crucial to obtain a smooth frequency response compatible with the SKA science cases. The design has also been driven by other factors such as the large-volume production (more than 130 000 antennas will be built) and the environmental conditions of the harsh Australian desert. A specific verification approach based on both wideband radiometric spectral and spatial measurements in relevant laboratory and in-situ conditions has been developed. Electromagnetic analyses and experimental results exhibit a very good agreement. In December 2019, this antenna was part of the reference solution for the System Critical Design Review of the SKA.

INDEX TERMS Log periodic antennas, low-frequency aperture array, radio astronomy.

I. INTRODUCTION

THE SQUARE Kilometre Array (SKA) will be the most sensitive radio telescope ever built. It will consist of two different instruments, one operating at low frequencies (50 – 350 MHz) and one at higher frequencies (0.35 – 15.35 GHz), located in Western Australia and South Africa respectively. These radio telescopes are conceived to make breakthrough discoveries in several areas of astronomy [1].

The SKA low-frequency instrument (SKA1-Low) will be deployed in the Murchison Radio-astronomy Observatory (MRO) in the Australian desert and will consist of an array with 131 072 antennas grouped in 512 stations [2]. Each station, which is an antenna array itself, is composed of 256 antennas randomly distributed within a circular area having a maximum distance between the antenna centers of 38 m. The antennas in a station are placed over a ground plane. The ground plane aims at minimizing the variability in the electrical characteristics of the terrain caused by the humidity conditions and the local terrain properties [3]. No mechanical movement of the antennas is required in order to steer the station beams, since they will be electronically tilted by varying the delays of each antenna element signal in the station digital beam-former.

This work is licensed under a Creative Commons Attribution 4.0 License. For more information, see https://creativecommons.org/licenses/by/4.0/

One of the challenging aspects of the SKA1-Low project is the design of an active array element satisfying severe dimensional, spatial and spectral requirements in a 7:1 frequency band [4]. Furthermore, such an antenna should operate over a conductive ground plane without being impaired by the latter intrinsic frequency-dependent scattering contribution. As well known, an omnidirectional element will show a null in the radiation pattern when placed at $\lambda/2$ from a ground plane. For this reason, more directive elements were developed from both the Vivaldi [5], [6], and the log-periodic antenna configuration [7]–[9]. The latter, also called SKA Log-periodic Antenna (SKALA, [7]) has shown better performance as far as mitigation of the frequency-dependent ground plane effects is concerned, i.e., residual frequency ripple on directivity, due to its higher front-to-back ratio with respect to the Vivaldi solution.

The number of array elements in a station (256) and the station diameter (38 m) impose a maximum footprint in the element size. This in turn produces severe limitations in the low-frequency performance. To overcome such limitations, the SKALA antenna configuration exploits a bow-tie dipole as bottom radiator for better impedance matching, while the ground plane itself enhances the directivity at low-frequencies [8], [9]. The ground plane cancellation phenomena at higher frequencies (i.e., when distance of the active region from the ground plane approach $\lambda/2$) are instead mitigated by the high front-to-back ratio (up to 30 dB) of the log-periodic configuration.

As shown in [10], the small element size of the bottom dipoles produces a frequency-dependent reactive antenna impedance at low-frequencies. Such a variation, combined to the Low Noise Amplifier (LNA) scattering parameters, can produce narrow peaks in the active antenna response (i.e., transducer gain, see Section II). The presence of such peaks has a major impact in the 21-cm cosmology experiments such as the Cosmic Dawn and the Epoch of Reionization [10].

The design and development approach reported in this paper is mainly focused to the achievement of a smoother spectral performance of the SKALA configuration. This objective has been obtained by designing an antenna element with a 50-ohm single-ended feeding. This is a remarkable difference with respect to previous versions of the SKALA antenna [7]–[9] as well as to other wire antennas used in low-frequency aperture-array radio telescopes such as LOFAR [11] and MWA [12], which all adopted a differential feed and higher impedance. The 50-ohm single-ended feeding allowed a fruitful co-design between antenna and LNA based on measured S-parameters. It should be pointed out that LNA characterization (especially in terms of noise parameters) can be directly carried out with standard measurement equipment in case of 50-ohm single-ended terminations only. The particular mounting configuration for the LNA has also been conceived to achieve a high consistency between simulations and measurements and a high degree of testability for a large number of array elements. Such a consistency between simulated and measured response has been verified with broadband radiometric spectral measurements both in anechoic chamber and in radio frequency quite environment (Murchison region) showing excellent results.

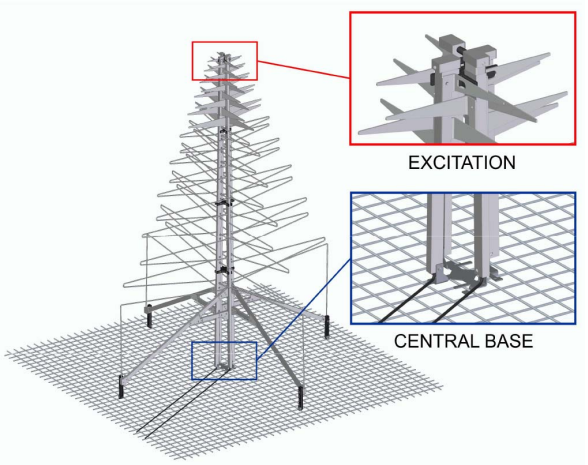

FIGURE 1. 3D CAD of the antenna with ground plane. The black parts (spacers and lateral feet) are made of nylon. The insets on the right show the two crossed feeding lines on top of the antenna, and the base of the antenna with the two output coaxial cables.

This paper is organized as follows: Section II describes the antenna requirements and the design challenges to achieve a 50-ohm SKALA design with smooth frequency behavior. The simulated performance and the validation approach are presented and discussed in Sections III and IV, respectively. Finally, Section V draws some conclusions and future work.

II. REQUIREMENTS AND DESIGN APPROACH

The antenna design has been driven by the top-level scientific requirements of the radio telescope flowed down to technical constraints [4]. The main RF performance of the antenna system are summarized in: *i*) frequency band from 50 to 350 MHz; *ii*) dual-linear polarization; *iii*) directivity at zenith around 8 dBi; *iv*) smooth directivity degradation within the Field of View (FoV, ±45 deg from zenith) with a drop-off of 3 dB with respect to the zenith; *v*) spectral smoothness of the antenna response [10]; *vi*) station Intrinsic Cross-Polarization (IXR) [13] higher than 15 dB, or at least than 12 dB (between 50 and 250 MHz) and 11 dB (above 250 MHz) within the FoV; *vii*) amplifier included in the antenna with $>$40 dB gain and a noise figure $<$1 dB in 50 – 100 MHz and $<$0.5 dB in 100 – 350 MHz. Another constraint on the antenna was a limited physical dimension, which resulted in a maximum length in the horizontal plane equal to 1.6 m, corresponding to $\sim\lambda/4$ at 50 MHz, and a total height around 2 m for maintenance reasons. Furthermore, several additional requirements such as the extreme environmental conditions, the manufacturing cost, the transportability to the final remote site, and the lifespan have been considered during the antenna development.

The antenna is formed by two identical Log Periodic dipole arrays orthogonally arranged in order to receive two linear polarizations (Fig. 1). The dipole feeding lines consist

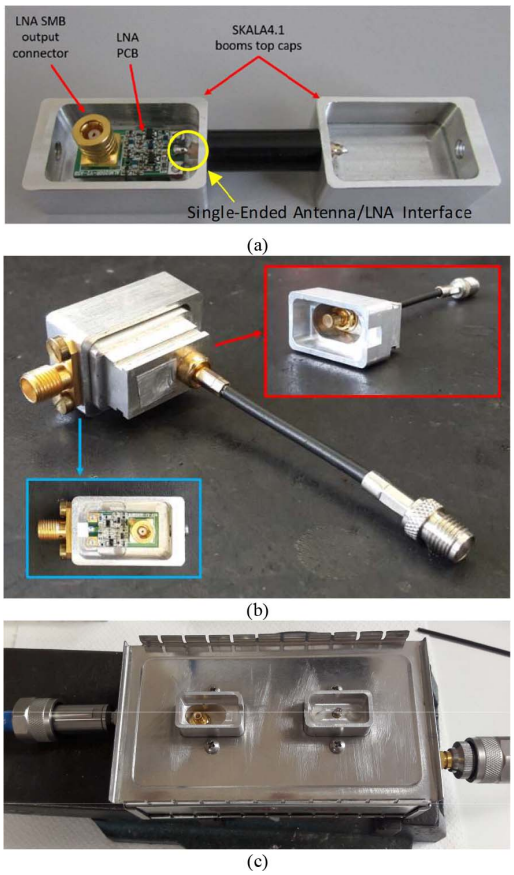

FIGURE 2. (a) Assembly of the two top caps with the LNA integrated (each antenna mounts two identical top cap assemblies, one for each polarization). The single-ended LNA/antenna interface is highlighted with the yellow circle. (b) LNA housing with single-ended setup for lab measurements with separate views on the 50-ohm input (light blue rectangle) and output (red rectangle) ports. (c) External setup for the acceptance test of the top cap assembly with single-ended connections to the Vector Network Analyzer.

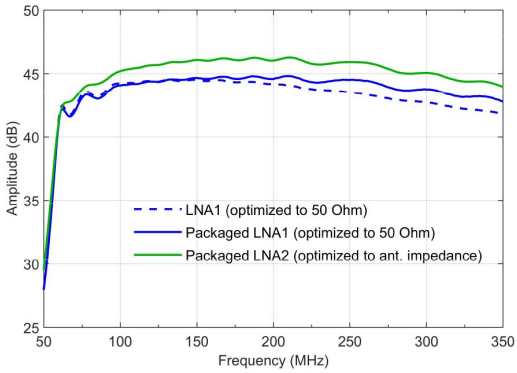

FIGURE 3. Transducer gain of two LNA designs in packaged and board-only conditions. All the curves have been obtained from measured data.

of four central rectangular tubes, also referred as "boom". The bottom dipole is based on a reinforced bow-tie shape to improve both the low frequency performance and the overall robustness, minimizing the lateral dimensions. The other dipoles are implemented as a combination of wire triangular dipoles screwed on the boom at low frequencies and solid triangles at high frequencies. The triangular shape has been selected in order to increase both the antenna directivity and the front-to-back ratio [14]. The number of solid (10) versus wire (10) dipoles results from a trade-off between electromagnetic (directivity) and mechanical (wind resistance) performance.

The central base (see bottom inset in Fig. 1) allows DC grounding of the antenna protecting the LNA against electrostatic discharge and indirect lightning. The antenna grounding has been taken into account in the overall design, although it has a marginal effect because the RF currents are mostly distributed in the active region of the antenna, without reaching the bottom junction.

On top of the antenna, two pairs of metal caps close the boom integrating also the LNA boards (one of them is visible inside the left cap shown in Fig. 2(a)). The LNA board ground is connected to the metal cap on the left of Fig. 2(a), while the microstrip LNA input is connected to the metal cap on the right by means of small metal cylinder embedded in an insulator made of acetal resin.

When the cap assembly is mounted on the antenna, the SMB LNA output connector is plugged into a corresponding connector mounted inside the antenna boom in a reliable and quick fashion. The coaxial cable is located inside the antenna boom down to the antenna base where either an output connector or an additional cable length exiting the antenna can be mounted. This configuration does not require a balun component to match the balanced antenna to the unbalanced coaxial port of the LNA because the shielded cable inside the antenna boom does not produce neither radiation nor coupling to the dipole feeding line (external part of the boom) [15]. The coaxial single-ended LNA/antenna electric interface is highlighted with the yellow circle in Fig. 2(a). It completely separates the antenna environment from the guided environment, i.e., LNA circuit and its output cable inside the boom. Full-wave simulations and measurements conducted with such a coax excitation have shown the same performance obtained with ideal (simulated) differential excitation. In particular, no appreciable asymmetry of the *E*-plane radiation pattern has been observed.

As reported in the Introduction, the single-ended solution has been selected to allow both antenna and LNA characterization with standard measurement equipment. Two measurement setups have been conceived and manufactured in order to measure the LNA in its mounting conditions (Fig. 2(b)) and to perform the final acceptance test before the integration on the antenna (Fig. 2(c)). Both antenna and packaged-LNA measurements have been crucial in refining the double-stage LNA design performed and produced by the industrial partner ASB Inc. (South Korea). As a custom product for this application, a low noise (noise figure equal to 0.53 dB at 200 MHz) amplifier module (ALN0200R) with high linearity over the frequency range from 50 to 350 MHz has been developed. It should be also noted that having such a simple measurement configuration is a leading factor to perform LNA acceptance tests in view of a large-volume production. The

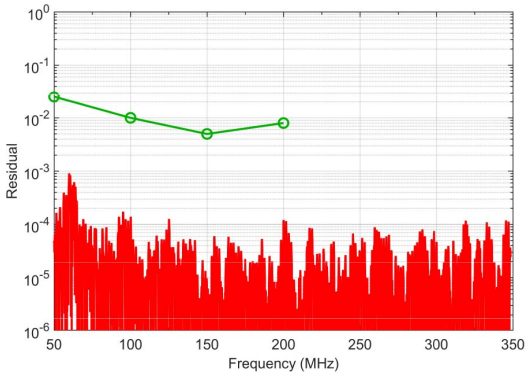

FIGURE 4. Smoothness performance (red curve) computed from the criterion in [10]. The scientific requirement is plotted in green.

outcome of such a co-design process is demonstrated in Fig. 3 and with the measured spectral responses in Section IV. Figure 3 shows the transducer gain of the LNA with the input port connected to the antenna impedance $G_T = |S_{21}^{LNA}|^2(1-|S_{11}^{ANT}|^2)/|1-S_{11}^{LNA}S_{11}^{ANT}|^2$, where S_{ij} are the scattering parameters of LNA and antenna. All the curves are computed from measured S-parameters. The blue lines show the performance of an LNA optimized for 50-ohm input impedance in both board-only and packaged conditions (Fig. 2(b)). The effect of packaging is definitely appreciable above 150 MHz. The ripple of less than ±0.4 dB from 70 to 100 MHz is instead due to the antenna mismatch (see Section III). The impact of such a ripple has been evaluated using the smoothness criterion described in [10], which is based on a 3rd-order local polynomial fitting of the frequency response. The computed residuals are shown in Fig. 4 with the red curve along with the scientific requirement in green. Such residuals are more than one order of magnitude below the requirements and at least one order of magnitude less than other antenna designs reported in [10]. Fig. 3 also reports a second LNA version (green curve) that has been further optimized to achieve a smaller ripple even in presence of the antenna mismatch. The benefit below 100 MHz is apparent.

A good antenna matching to a 50-ohm reference impedance has been achieved by proper selection of boom size (rectangular section, 25 × 15 mm) and spacing (from 23.5 (top) to 95.4 mm (bottom)). On the other hand, such a boom configuration with narrow spacing produces a significant guided coupling not only to the active region of the log-periodic (i.e., group of dipoles close to λ/2) but also to the bottom dipoles whose length is multiple of λ/2 [16], [17]. The latter produce glitches in the directivity frequency response shown in Fig. 5, computed with FEKO [18]. To mitigate such an effect, a high number of dipoles (20) and a slight boom opening angle (also visible in Fig. 1) have been exploited. The former aspect allows a smooth transition among dipoles with different discrete lengths, while the latter slightly increases the intrinsic radiation of the transmission line (dipole feeding) with a consequent reduction of the spurious coupling to the bottom dipoles. The parametric analysis with different opening

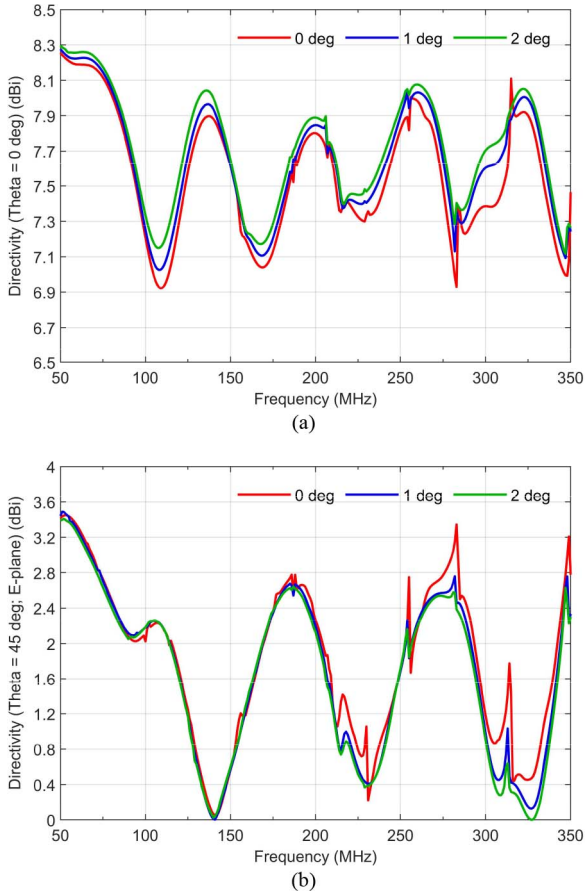

FIGURE 5. Directivity of the 50-ohm single-ended antenna for different values of the boom opening angle at two zenith angles: (a) 0 deg and (b) 45 deg on the *E*-plane.

angles reported in Fig. 5 shows that a boom opening angle of 1 deg already produces a significant improvement with respect to the straight parallel boom, whereas a marginal improvement can be observed from 1 to 2 deg.

Finally, for the antenna material the aluminum (anticorodal alloy) was selected after a comparative analysis against stainless and mild steel. The outcome of this analysis, supported also by a 200-h salt spray test on different aluminum alloys and joint assemblies for evaluating the corrosion resistance, showed that the aluminum was the optimal solution thanks to the: *i)* excellent electrical characteristics, *ii)* lightness (ensuring the same stiffness) which means lower shipment costs, easier handling and installation, *iii)* no surface treatment required and *iv)* lower cost.

III. NUMERICAL RESULTS

Different EM commercial simulators, mainly based on the Method of Moments (MoM) technique, have been used for the numerical analysis of the antenna. The "as-built" model of the antenna shown in Fig. 1 has been simplified removing mechanical details, such as bolt, screws, access holes, small plate structures, without any impact on the EM performance reaching a final model with around 10 000 degrees of freedom. This leads to a computational time for FEKO in a multi-core workstation (2 x AMD EPYC 7301, RAM

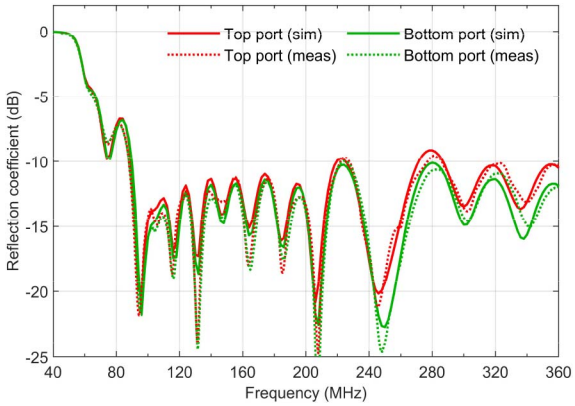

FIGURE 6. Simulated (continuous line) and measured (dashed line) reflection coefficient for the two antenna ports in the frequency range 40 – 360 MHz. The reference impedance is 50 ohm.

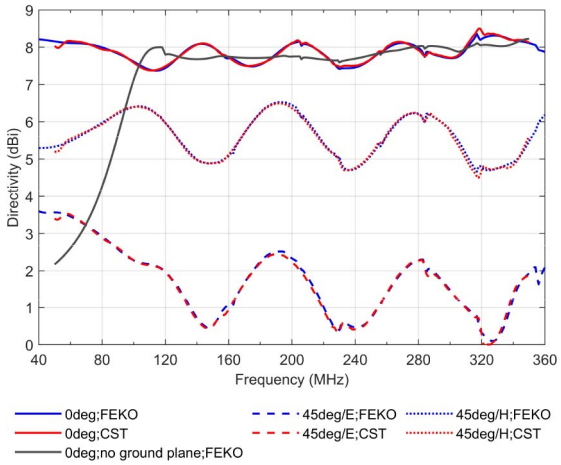

FIGURE 7. Directivity at zenith (solid curves) and at 45 deg off-zenith for both principle planes (dotted curves in *H*-plane and dashed curves in *E*-plane) in the frequency band 40 – 360 MHz with 1 MHz frequency resolution computed with FEKO (blue) and CST MWS (red). The grey curve represents the antenna directivity at zenith without ground plane.

512 GB) of few minutes for each frequency point. The simulations have been conducted with the antenna lying over an infinite horizontal perfect electric conductor solid plane and applying the reflection coefficient approximation.

The computed antenna reflection coefficient is plotted in Fig. 6 for the two polarizations between 40 and 360 MHz. The two ports, which are 1 cm apart along the vertical direction (see top inset of Fig. 1), present a slightly different matching, the bottom port being more matched at 50 ohm than the top port. The largest difference in the reflection coefficient between the two polarizations occurs above 200 MHz, where the antenna is well matched (better than −9 dB) and therefore this is not expected to produce significant unbalance between the two channels. The reflection coefficient suffers at low frequencies for the limited physical length of the bottom dipoles, which results in a matching at 50 MHz equal to −0.2 dB. The effect of the mismatch at low frequency on the antenna performance is discussed in more details in Section IV.

Figure 7 shows the directivity of the designed antenna across frequency both at zenith and at the edges of the FoV in the two principal planes. The average of the zenith directivity across frequency is 7.9 dBi with a maximum peak-to-peak of 1 dB. The slow ripple (about 60 MHz period) is determined by the antenna back-lobe reflected from the ground plane towards the sky (front-to-back ratio higher than 20 dB for frequencies above 100 MHz, and higher than 25 dB above 130 MHz). Below 100 MHz, the antenna exploits the ground plane, which acts as an electromagnetic reflector to achieve the required directivity towards the zenith (the response of the antenna without ground plane is shown by the grey curve in Fig. 7). The transition between these two operative conditions has been achieved without discontinuities in the frequency response.

As described in Section II, small glitches characterized by a peak-to-peak amplitude in the range of 0.1-0.2 dB and with a bandwidth of less than 1 MHz are present in the directivity frequency response. The same peaks are present in the free-space simulation of the antenna (grey curve in Fig. 7). This confirms that these peaks are an intrinsic characteristic of the antenna, i.e., they are not related to the ground plane. It should be pointed out that both FEKO and CST MWS [19] simulations are shown in Fig. 7 with very good agreement. The time-domain CST solver based on the finite integration technique required 60 mesh line/wavelength and a −50 dB energy decay threshold to visualize the small glitches.

The drop in the off-zenith directivity (Fig. 7) is generally less than 3 dB in the *H*-plane, while in the *E*-plane it is higher (up to 8 dB) reducing the sensitivity of the radio telescope at low elevations in the corresponding azimuth directions.

For the polarization aligned to the *y*-direction, Fig. 8 shows for three frequencies (50, 200 and 350 MHz) a *uv*-map of the (amplitude) co-polar directivity in the whole semi-hemisphere above the horizon. The ellipticity of the beam, which is evident from these maps, is quantified in a Half Power Beam Width equal to 74 (*E*-plane) and 92 deg (*H*-plane) at 50 MHz, and 56 (*E*-plane) and 92 deg (*H*-plane) at 350 MHz. The maps of Fig. 8 also include the directions of the electric field. Due to the intrinsic geometry of the Log Periodic antennas, a slight rotation of the *E*-plane with respect to the main geometrical axis is visible, maximum tilt being 6 deg at 50 MHz. However, a similar rotation is present also for the other polarization, maintaining therefore at every frequency the orthogonality between the *E*-planes of the two polarizations.

Furthermore, the radiation efficiency of the antenna has been computed using an electrical conductivity for the aluminum equal to 1.4E7 S/m. This value has been found by a parametric simulation analysis aimed at matching the measured transmission coefficient of a 1-m long coaxial cable made with the same antenna material. The computed radiation efficiency has a very flat behavior above 64 MHz (>99%), while it decreases at the lowest operating frequency (50 MHz) to 90%.

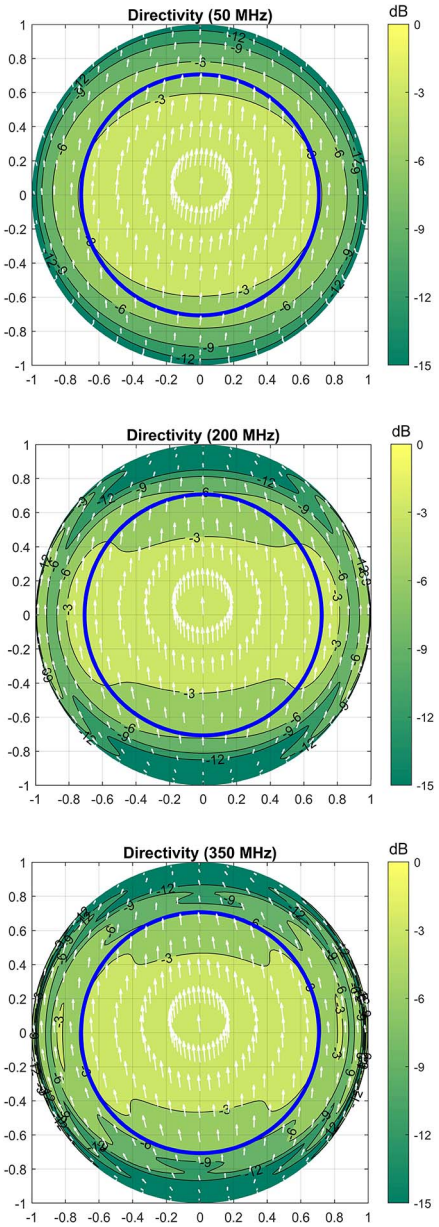

FIGURE 8. *uv*-maps of the normalized co-polar directivity for *y*-polarization at 50, 200 and 350 MHz. The blue circle indicates the edge of the FoV. The white arrows show the direction of the amplitude of the electric field.

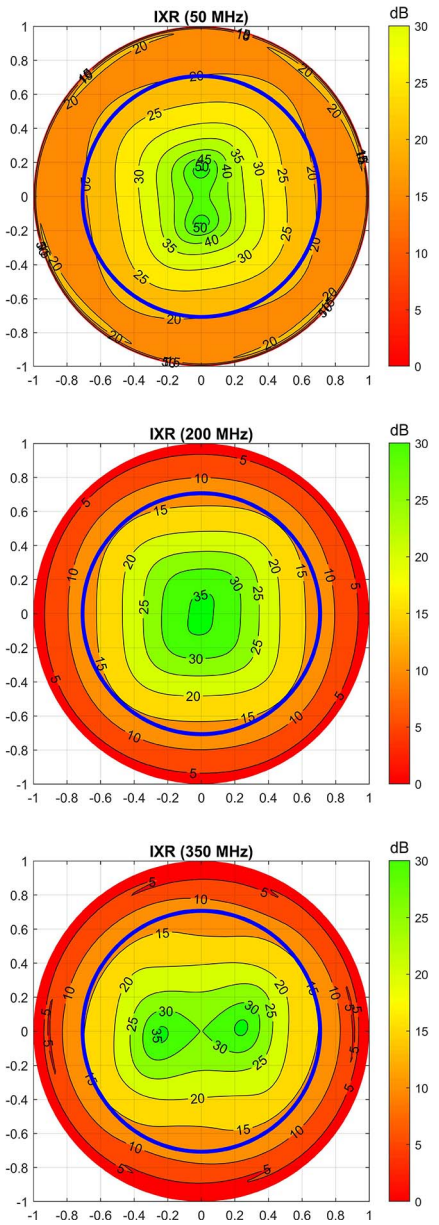

FIGURE 9. *uv*-maps maps of the IXR for *y*-polarization at 50, 200 and 350 MHz. The color map has been saturated to highlight low IXR values. The blue circle indicates the edge of the FoV.

The final simulated results show the antenna IXR performance, which quantifies the orthogonality of the two channel transfer functions regardless of the adopted reference system [13]. The maps reported in Fig. 9 show the IXR in *uv*-coordinates for three different frequencies, with the blue circle indicating the edge of the FoV. The polarization purity performance is higher at zenith and deteriorates moving towards lower elevations. At high frequency, the IXR values are lower than 15 dB at low elevation (around 35-40 deg from zenith). As discussed in [20], the IXR already results in less than 15 dB for two ideal crossed dipoles with a pattern asymmetry between the two principle planes reaching 4 dB. Therefore, two other more tolerant thresholds are considered acceptable as they do not cause any major science impacts: 12 dB (between 50 and 250 MHz) and 11 dB (above 250 MHz). In conclusion, only at 50 MHz, the IXR is always above 15 dB in the entire FoV, while at 200 and 350 MHz it matches the limits given by the major science impact.

IV. EXPERIMENTAL VALIDATION

Several antenna prototypes have been built and tested in order to experimentally assess the validity of the design approach.

The measured reflection coefficients on a prototype antenna placed outdoor over a finite 3 x 3 m^2 ground

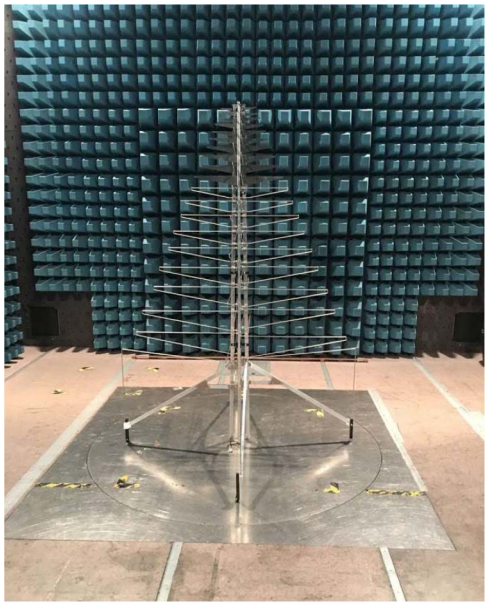

FIGURE 10. Antenna under test in a semi-anechoic chamber. The dimensions of the chamber (9.10 x 5.80 x 5.55 m) are not adequate for measuring the antenna pattern. The main purpose of the chamber is to embed the antenna in a RF quite environment, where the absorbing walls act as a blackbody emitting at room temperature.

plane is shown in Fig. 6. The test has been performed by substituting the LNA board shown in Fig. 2(a) with a pass-through. For both ports, the agreement between simulations and measurements is fully satisfactory.

Spectral (radiometric) measurements of the noise power received by the antenna connected to the LNA have been conducted in two different radio-quiet environments: a semi-anechoic chamber (see Fig. 10) and an isolated installation of the antenna at MRO. The former is similar to the hot-load configurations adopted for aperture-array calibration and sensitivity measurements above 400 MHz in [21]–[23]. In this paper, as a novel aspect, such a constant temperature blackbody is instead used to accurately verify the consistency and smoothness of the frequency response down to 20 MHz. It should be noted that the possibility of accurately testing low-frequency antennas in a shielded indoor environment is very useful and practical before conducting similar experiments in radio-quite very remote areas such as MRO.

The quantitative expression of the received power (P_{rec}) is given by:

$$P_{rec} = G_T T_{sys} B k G_{Rx} \tag{1}$$

where G_T is the transducer gain of the LNA with the input port connected to the antenna impedance (see Section II), B and k are the bandwidth (300 kHz) and the Boltzmann constant, respectively, and G_{Rx} is the receiver gain (including cables). Finally, T_{sys} is the system temperature given by:

$$T_{sys} = \eta_{rad} T_A + (1 - \eta_{rad}) T_{Ph} + T_{LNA} + \frac{T_{Rx}}{G_T} \tag{2}$$

where η_{rad} and T_A are the antenna radiation efficiency and the antenna noise temperature (integral of directivity multiplied by scene brightness temperature), respectively, whereas

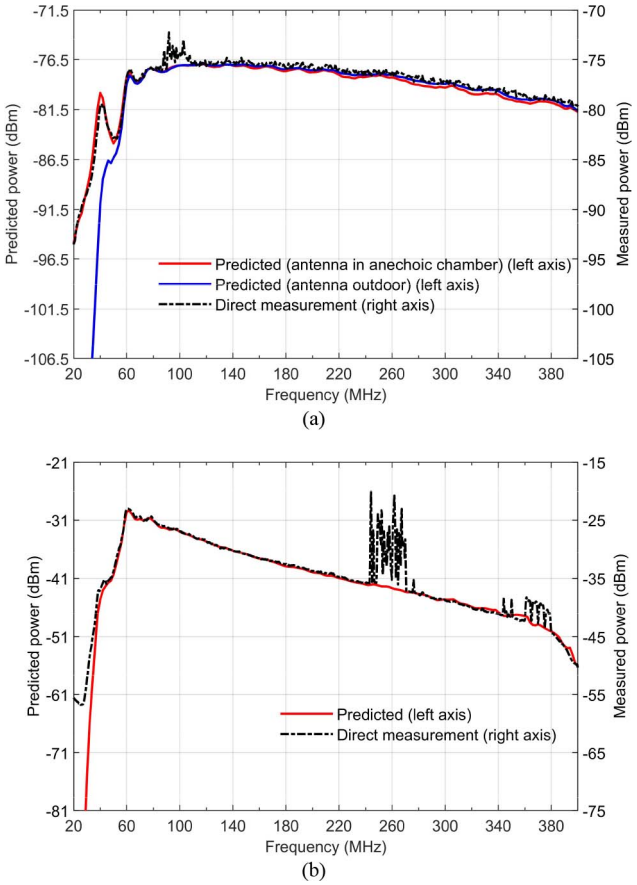

FIGURE 11. Direct and predicted measured power spectrum (bandwidth equal to 300 kHz) for the antenna connected to the LNA for two different installations: (a) in a semi-anechoic chamber and (b) at MRO site.

T_{Ph} is its physical temperature. T_{LNA} and T_{Rx} are the LNA and receiver equivalent noise temperatures, respectively.

The main difference in the two setups is the antenna temperature T_A which is constant (∼290 K) for the semi-anechoic chamber (the absorbers are considered as a uniform emitting blackbody at ambient temperature), while at the Australian site it is determined by the sky emission. The latter is mostly dominated by the galactic synchrotron emission and T_A can be approximated as $20(0.408/f[GHz])^{2.5}$ [24].

The measured responses are compared in Fig. 11 to the equivalent predictions produced by cascading the various device contributions according to (1). In particular, apart from antenna temperatures reported above, the measured device scattering and noise parameters were used for the predictions in Fig. 11 thanks the 50-ohm single-ended interfaces described in Section II. The predictions shown in Fig. 11(a) with red and blue curves have been computed according to the measured antenna reflection coefficients in the chamber and outdoor conditions, respectively. The former, which takes into account the impact of the higher reflection of the chamber absorbers on the antenna reflection coefficient below 60 MHz, shows a better agreement to the measured results (peak at 40 MHz). While the blue curve is expected to better reproduces the antenna response

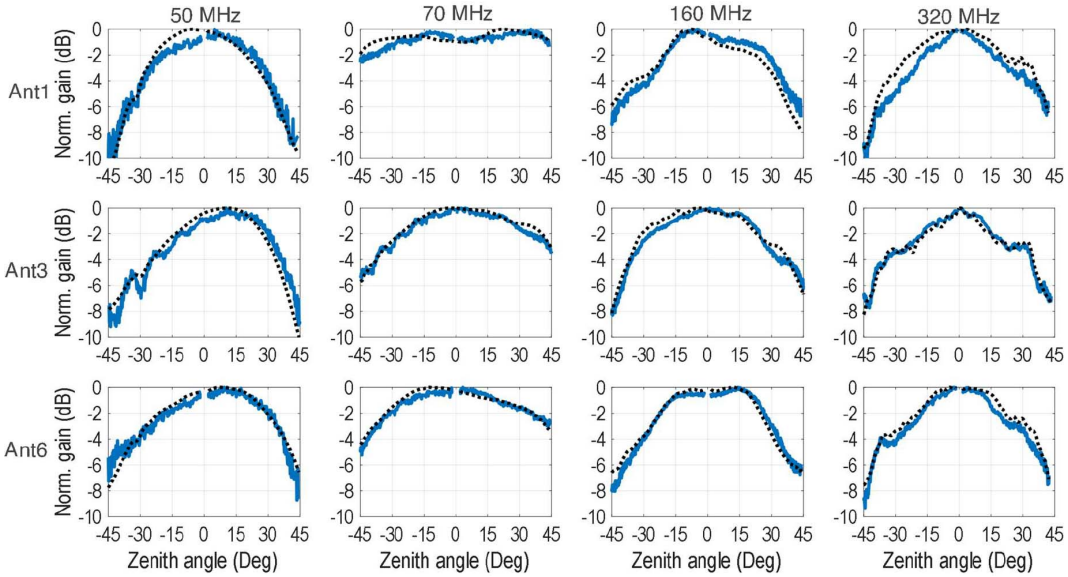

FIGURE 12. Normalized embedded element patterns of three antennas of AAVS1.5 (*y*-polarization) at 50, 70 MHz, 160 and 320 MHz. Columns refer to different frequencies, while rows to different array elements. Blue: measurements, dashed black: simulations.

in its operative conditions. The small offset of 1.5 dB between measured (right scale) and predicted curves (left scale) is consistent with the absolute accuracy of the spectrum analyzer used as receiver. Apart from some residual radio frequency interferences in the direct measurements (FM band), the agreement is very satisfactory showing a good reproducibility of the active antenna response also in low-matching conditions (below 60 MHz).

The same agreement level can be observed in Fig. 11(b) where the full receiving system of SKA1-Low has been exploited, i.e., optical fiber link, receiver (including digital step attenuator) and digital acquisition system [25]. The higher complexity of the receiver justifies the 6-dB difference in the predicted absolute values, i.e., the full receiver was not calibrated for absolute power. Fig. 11(b) shows a smooth high-pass frequency response without resonance peaks. The negative slope of the received power versus frequency (above 60 MHz) is different with respect to Fig. 11(a) because of the different antenna temperature spectrum (see above). The measured spectrum of Fig. 11(b) shows some interferences in the band 240-280 MHz and above 340 MHz. It should be noted that for both the indoor and in-situ measured frequency responses the consistency between measurements and simulation is within 0.5 dB. Such a good agreement has never been reported in the scientific literature for this key performance. With reference to Fig. 3, LNA1 has been used in both tests owing to its availability at that time.

The drop of received power below 60 MHz is due to the reduction of the transducer gain G_T, which is caused by the antenna mismatch. The impact of the 10 dB reduction of G_T from 60 to 50 MHz is negligible on the system noise temperature. With reference to (2), T_{Rx}/G_T is about 12 K at 50 MHz ($T_{Rx} = 12000$ K and G_T is about 30 dB) whereas T_A is around 4000 K due to sky emission.

The radiation patterns of the designed antenna have been measured by using an Unmanned Aerial Vehicle (UAV) equipped with a Real Time Kinematic (RTK) differential GPS and a tunable RF generator connected to a dipole [26]. This customized UAV system has been used for characterizing several low-frequency aperture array such as LOFAR [27] and previous SKA1-Low demonstrators [28]. The measurement campaign has been performed at MRO on the so-called Aperture Array Verification System (AAVS) version 1.5, which comprises 48 elements of the antenna described in this paper grouped in 3 different clusters of 16 antennas each [29]. The UAV performed linear scans at a constant height of 120 m to characterize the principal cuts of the radiation patterns with an angular coverage of ± 45 deg from zenith. The measured element patterns in Fig. 12 are affected by the mutual coupling between adjacent elements and therefore show some asymmetries and irregularities. However, these effects are fully captured by the numerical patterns obtained simulating the geometry of AAVS ver. 1.5 with Galileo EMT [30]. The comparison of the normalized patterns in the *E*-plane for three antennas and at four frequencies shown in Fig. 12 turns out to be very consistent.

As far as non-RF requirements are concerned, an important environmental test has been performed on a full-size prototype placed in the wind tunnel [31]. The tests were performed at increasing wind speed up to about 120 km/h to assess its structural deformation under wind load. The tip deflection of the antenna was about 4.4 deg in correspondence of the maximum wind speed equal to 123 km/h. In less severe conditions, i.e., up to 60 km/h the tip deflection was below 1 deg. Such a deflection will not produce significant degradation of the observation performance because of the relatively broad element patterns (see Fig. 12). A structural

mode analysis of the antenna is also reported in [31]. The antenna presents very high modal density, with several tens of modes within the first 25 Hz. The deformed shape assumed by the antenna is close to the first bending mode due to the transversal wind load on the solid triangular dipoles.

V. CONCLUSION

The active log-periodic antenna discussed in this paper matches the challenging RF requirements of the SKA1-Low project. It has been selected as the reference design during the SKA System Critical Design Review with the name of SKALA4.1. The key aspects of this solution are: the smooth spectral response; the antenna/LNA interface that allows a good degree of testability; a slightly open boom to mitigate the spurious resonances related to the small boom spacing; a high number of dipoles to satisfy the directivity requirement across frequency; a short-circuited grounding of the antenna for electrically protection of the LNA from electrostatic discharge; the choice of anticorodal aluminum for better electrical conductivity, lightness and cost with respect to other materials.

The antenna design has been intensively characterized through numerical EM simulations and experimental tests showing very consistent results. The obtained residual ripples in the transducer gain response of about ± 0.4 dB represent state-of-the-art for this kind of wideband antenna system.

The next step is the verification of a single station formed by 256 antennas. For this purpose, 256 antennas have been recently manufactured by Sirio Antenne (Italy) and installed at MRO (AAVS ver. 2.0). Besides EM simulations, measured spectral responses and radiation patterns, the astronomical tests will also provide key information on the actual performance of a full SKA1-Low station.

REFERENCES

[1] *Advancing Astrophysics With the Square Kilometre Array*, SKA Organisation, Macclesfield, U.K., 2015.
[2] M. G. Labate, P. Dewdney, R. Braun, M. Waterson, and J. Wagg, "The SKA low-frequency telescope: Performance parameters and constraints on the array configuration," in *Proc. 11th Eur. Conf. Antennas Propag. (EUCAP)*, Paris, France, Mar. 2017, pp. 2259–2263.
[3] A. T. Sutinjo *et al.*, "Characterization of a low-frequency radio astronomy prototype array in western Australia," *IEEE Trans. Antennas Propag.*, vol. 63, no. 12, pp. 5433–5442, Dec. 2015.
[4] M. G. Labate, L. Stringhetti, P. Dewdney, and R. Braun, "Next step in the aperture arrays and antenna design for the world's largest radio telescope of the future," in *Proc. Int. Conf. Electromagn. Adv. Appl. (ICEAA)*, Turin, Italy, Sep. 2017, pp. 1925–1928.
[5] G. Pupillo *et al.*, "Medicina array demonstrator: Calibration and radiation pattern characterization using a UAV-mounted radio-frequency source," *Exp. Astron.*, vol. 39, no. 2, pp. 405–421, Jun. 2015.
[6] P. Bolli *et al.*, "From MAD to SAD: The Italian experience for the low-frequency aperture array of SKA1-LOW," *Radio Sci.*, vol. 51, no. 3, pp. 160–175, 2016.
[7] E. de Lera Acedo, "SKALA: A log-periodic antenna for the SKA," in *Proc. Int. Conf. Electromagn. Adv. Appl. (ICEAA)*, Cape Town, South Africa, Sep. 2012, pp. 353–356.
[8] E. de Lera Acedo, N. Razavi-Ghods, N. Troop, N. Drought, and A. J. Faulkner, "SKALA, a log-periodic array antenna for the SKA-low instrument: Design, simulations, tests and system considerations," *Exp. Astron.*, vol. 39, no. 3, pp. 567–594, Oct. 2015
[9] E. de Lera Acedo, N. Drought, B. Wakley, and A. Faulkner, "Evolution of SKALA (SKALA-2), the log-periodic array antenna for the SKA-low instrument," in *Proc. Int. Conf. Electromagn. Adv. Appl. (ICEAA)*, Turin, Italy, Sep. 2015, pp. 839–843.
[10] E. de Lera Acedo *et al.*, "Spectral performance of SKA log-periodic antennas I: Mitigating spectral artefacts in SKA1-LOW 21 cm cosmology experiments," *Monthly Notices Royal Astron. Soc.*, vol. 469, no. 3, pp. 2662–2671, Aug. 2017.
[11] S. J. Wijnholds and W. A. van Cappellen, "In situ antenna performance evaluation of the LOFAR phased array radio telescope," *IEEE Trans. Antennas Propag.*, vol. 59, no. 6, pp. 1981–1989, Jun. 2011.
[12] S. J. Tingay *et al.*, "The Murchison widefield array: The square kilometre array precursor at low radio frequencies," *Publ. Astron. Soc. Aust.*, vol. 30, p. e007, Jan. 2013.
[13] T. D. Carozzi and G. Woan, "A fundamental figure of merit for radio polarimeters," *IEEE Trans. Antennas Propag.*, vol. 59, no. 6, pp. 2058–2065, Jun. 2011.
[14] E. de Lera Acedo *et al.*, "SKA-1- LOW antenna selection—Description of the LPD antenna candidates, LFAA antenna and LNA work package," document SKA Memo 20-02, SKA Org., Manchester, U.K., Aug. 2017. [Online]. Available: https://www.skatelescope.org/wp-content/uploads/2020/06/SKA1_LOW_Antenna_Selection_Aug2017.pdf
[15] D. Isbell, "Log periodic dipole arrays," *IRE Trans. Antennas Propag.*, vol. 8, no. 3, pp. 260–267, 1960.
[16] Z.-L. Gong and K. G. Balmain, "Reduction of the anomalous resonances of symmetric log-periodic dipole antennas," *IEEE Trans. Antennas Propag.*, vol. 34, no. 12, pp. 1404–1410, Dec. 1986.
[17] M. Hilbert, M. A. Tilston, and K. G. Balmain, "Resonance phenomena of log-periodic antennas: Characteristic-mode analysis," *IEEE Trans. Antennas Propag.*, vol. 37, no. 10, pp. 1224–1234, Oct. 1989.
[18] *Altair Feko Overview*. Accessed: Jun. 10, 2020. [Online]. Available: https://altairhyperworks.com/feko/
[19] *Electromagnetic Field Simulation Software*. Accessed: Jun. 10, 2020. [Online]. Available: https://www.3ds.com/products-services/simulia/products/cst-studio-suite/
[20] B. Fiorelli, M. Arts, G. Virone, E. de Lera Acedo, and W. A. van Cappellen, "Polarization analysis and evaluation for radio astronomy aperture array antennas," in *Proc. 7th Eur. Conf. Antennas Propag. (EuCAP)*, Gothenburg, Sweden, Apr. 2013, pp. 461–465.
[21] Y. Zhang and A. K. Brown, "Noise temperature measurement of finite compact aperture array," in *Proc. Int. Conf. Electromagn. Adv. Appl. (ICEAA)*, Torino, Italy, 2013, pp. 1029–1031.
[22] E. E. M. Woestenburg, L. Bakker, M. Ruiter, M. V. Ivashina, and R. H. Witvers, "THACO: A test facility for characterizing the noise performance of active antenna arrays," in *Proc. 8th Eur. Radar Conf.*, Manchester, U.K., 2011, pp. 389–392.
[23] A. P. Chippendale *et al.*, "Measured aperture-array noise temperature of the mark II phased array feed for ASKAP," in *Proc. Int. Symp. Antennas Propag. (ISAP)*, Hobart, TAS, Australia, 2015, pp. 1–4.
[24] G. C. Medellín, "Antenna noise temperature calculation," in *SKA Memo Series 95*. Macclesfield, U.K.: SKA Org., Aug. 2007.
[25] G. Naldi *et al.*, "The digital signal processing platform for the low frequency aperture array: Preliminary results on the data acquisition unit," *J. Astron. Instrument.*, vol. 6, no. 1, 2017, Art. no. 1641014.
[26] G. Virone *et al.*, "Antenna pattern verification system based on a micro unmanned aerial vehicle (UAV)," *IEEE Antennas Wireless Propag. Lett.*, vol. 13, pp. 169–172, 2013.
[27] G. Virone *et al.*, "Strong mutual coupling effects on LOFAR: Modeling and in situ validation," *IEEE Trans. Antennas Propag.*, vol. 66, no. 5, pp. 2581–2588, May 2018.
[28] E. de Lera Acedo *et al.*, "SKA aperture array verification system: Electromagnetic modeling and beam pattern measurements using a micro UAV," *Exp. Astron.*, vol. 45, no. 1, pp. 1–20, Mar. 2018.
[29] D. B. Davidson *et al.*, "Electromagnetic modelling of the SKA-LOW AAVS1.5 prototype," in *Proc. Int. Conf. Electromagn. Adv. Appl. (ICEAA)*, Granada, Spain, 2019, pp. 1032–1037.
[30] *A Comprehensive Set of Modeling and Simulation Products Designed for Electromagnetic Engineering (EME) Applications*. Accessed: Jun. 10, 2020. [Online]. Available: https://www.idscorporation.com/pf/galileo-suite/

[31] G. Iuso, G. Virone, G. Cafiero, E. Bonisoli, D. Lisitano, and S. Venturini, "Aeroelastic-structural coupling in antenna prototype for windy open-space," in *Proc. VIII Int. Conf. Comput. Methods Coupled Problems Sci. Eng.*, Barcelona, Spain, Jun. 2019, pp. 481–492.

PIETRO BOLLI received the Laurea degree in electronic engineering and the Ph.D. degree in computer science and telecommunications engineering from the University of Florence, Italy, in 1999 and 2003, respectively. In 2002, he started his professional career as a Microwave Engineer at the Italian National Institute for Astrophysics (INAF) conducting research in the field of technology applied to radio astronomy. He is currently a Technologist at the INAF Arcetri Astrophysical Observatory, where he is involved in the design, characterization, and calibration of the low frequency instrument of the Square Kilometer Array. P. Bolli is the Italian responsible for the protection of the frequency bands used by radio astronomers and represents INAF in the Committee on Radio Astronomy Frequencies (CRAF). He is also Officer of the Commission J (Radio Astronomy) of the Italian Committee of the Union Radio Scientifique Internationale (URSI). He is co-author of about 140 scientific publications, which have appeared in international referred journals and conferences.

LORENZO MEZZADRELLI was born in Mantova, Italy, in 1977. He received the M.Sc. degree in telecommunications engineering from the University of Bologna in 2004. Since 2004, he has been working in the R&D Department, SIRIO Antenne as an Antenna Designer and Project Manager. His activities are focused on design of base station and mobile antennas from 27 MHz to 6 GHz. With Sirio Antenne, he is working on the Square Kilometre Array project (SKA), in particular on SKA-low antenna electrical and mechanical design.

JADER MONARI received the degree in electronic engineering from the University of Bologna in 1996 with an experimental thesis at the CNR (now INAF) Radioastronomy Institute. In 1997, he joined the Sky Polarization Observatory(SPOrt) project. During 2003, he worked on the design of new single-feed/multi-feed/multi-frequency architectures for the receiving systems of the 64-m Sardinia Radio Telescope. In 2004, he started a collaboration within Square Kilometer Design Studies (SKADS). In particular, he worked at the design of BEST receiver architecture (Italian Test Bed for SKA) and for the EMBRACE receiver (Dutch SKA pathfinder planar Aperture Array). He was a member of the PREPSKA team since 2008 as liaison engineer and he became program coordinator for the Italian AAlow task part of Aperture Array Verification Program (AAVP) then named Aperture Array Design Consortia (AADC). Within AADC he was appointed as a Task Leader for receivers. Still within the framework of international programs, he coordinates the technical resources for the development of the new receiving system for LOFAR2. Nowadays he is the Italian Program Manager for all SKAlow tasks and, at an international level, part of the executive board that coordinates all the activities of this bridging phase. He is also part of the SKA and LOFAR Italian board appointed by the Scientific Directorat ae. He has been Medicina Radiotelescope station manager for seven years now.

FEDERICO PERINI was born in Bologna, Italy, in 1974. He received the Laurea degree in telecommunications engineering (summa cum laude) from the University of Bologna in 2001. From 2002, he has worked for the Institute of Radio Astronomy of National Institute for Astrophysics (INAF) at the Medicina radio telescopes as a RF project engineer. His activities are focused on the design and development of analogue receiver chains for both the Italian radio telescopes (Northern Cross Array, VLBI 32m dishes of Medicina and Noto and Sardinia Radio Telescope) and for international low frequency instruments and/or projects like the forthcoming Square Kilometre Array (SKA-Low) and LOFAR2.0. His expertise covers Low Noise Amplifier (LNA), RF/IF receivers and signal transportation systems based on RFoF (RF over Fibre) technology.

ALBERTO TIBALDI (Member, IEEE) was born in Casale Monferrato, Italy, in 1987. He received the B.Sc., M.Sc., and Ph.D. degrees in electronic engineering from the Polytechnic of Turin, in 2009, 2011 and 2015, respectively. From 2012 to 2019, he was with the Italian National Council of Research (CNR) as a Research Fellow. Since 2019, he has been with the Department of Electronics and Telecommunications, Polytechnic of Turin as an Assistant Professor, where he teaches courses on semiconductor devices and numerical analysis. His scientific interests mainly regard the multi-physics modeling of optoelectronic devices.

GIUSEPPE VIRONE (Member, IEEE) was born in Turin, Italy, in 1977. He received the degree in electronic engineering (summa cum laude) and the Ph.D. degree in electronics and communication Engineering from the Politecnico di Torino, Italy, in November 2001 and 2006, respectively. He is currently a Researcher at the Istituto di Elettronica e di Ingegneria Informatica e delle Telecomunicazioni (IEIIT), Italian National Research Council (CNR). He joined IEIIT as a Research Assistant in 2002. He coordinated more than 15 scientific projects funded by both the industry and other scientific research organizations and joined more than 30 research projects as a collaborator. He authored 43 journal papers, 134 conference papers, and 3 European patents. His activities concern the design, numerical analysis, and characterization of microwave and millimeter waveguide passive components for feed systems, antenna arrays, frequency selective surfaces, compensated dielectric radomes, and industrial sensing applications.

MIRKO BERCIGLI was born in Florence, Italy, in 1973. In 2000, he received the Laurea degree in electronic engineering from the University of Florence. Since September 2000, he has been employed in the Computational Electromagnetic Laboratory, IDS Ingegneria dei Sistemi S.p.A., as a System Analyst in the field of electromagnetism. He is currently the head of the "Computational Electro Magnetic Engineering." Since 2000, he has participated in IDS projects in the field of applied electromagnetism, at first as an Analyst and then as a Project Leader. From the technical point of view, he experienced activities on the following topics: CAE tools design for electromagnetic applications, electromagnetic methods development and acceleration, and antenna siting analysis on various platforms (naval, airborne, earthbound, and spaceborne). He co-operates with several research centers such as the University of Florence, the Politecnico of Turin, the University of Pisa, the University of Siena, the University of l'Aquila, and the University of Rome in developing e.m. numerical methods. He also participated in several international programs supported by European Space Agency (ESA) and European Community (EC).

LORENZO CIORBA was born in Avezzano, Italy, in 1993. He received the master's degree (110/110) in mathematical engineering from Politecnico di Torino, Italy, in March 2018, with the thesis "Hybrid Antenna Measurement and Simulations" with Prof. G. Vecchi as a supervisor. In June 2018, he joined the Applied Electromagnetics and Electronic Devices Group of the Institute of Electronics, Computer and Telecommunication Engineering (IEIIT), Italian National Research Council (CNR), as a Research Fellow. From November 2019, he has been a Ph.D. student in electrical, electronics and Communications Engineering at Politecnico di Torino. His scientific interests regard computational electromagnetics and characterization of antennas, in particular UAV-based near field antenna measurements.

PAOLA DI NINNI received the physics degree in astrophysics and space physics at the University of Florence, Italy, in 2008, and the Ph.D. degree in experimental physics from the University of Siena, Italy, in 2017. From 2009 to 2013, she worked at the Department of Physics and Astronomy, University of Florence, Italy. She currently works as a Grant Researcher in Radio Astronomy at the Arcetri Astrophysical Observatory, National Institute of Astrophysics, Italy. Her research interests mainly focus on electromagnetic theory, antennas, and radio telescopes.

MARIA GRAZIA LABATE received a master's degree (summa cum laude) in telecommunication engineering from the "Mediterranea" University of Reggio Calabria, Italy, in 2008 and a Ph.D. degree in electronic engineering from the Second University of Naples, Italy, in 2011. In 2008, she worked as a System Integration & Technology Analyst for Accenture S.p.A, and joined the R&D division of Optel InP (at SELEX S.I.) as Phased Array Antenna Designer & Electromagnetic Field Expert. During 2009—2013, she worked as a Radar Antenna Designer & System Analyst in the Innovation Team of SELEX Sistemi Integrati S.p.A., a Finmeccanica Company, where she was the recipient of the "Innovation Award" in 2010. She joined the Antenna Centre of Competence of Astrium Ltd. (EADS) in 2013, and later took part in the SKA Project. She is currently working at the Headquarters of the Square Kilometre Array (SKA) Organisation, which is the entity responsible for overseeing the global activities and international effort to eventually build the world's largest radio telescope. She joined the SKA Organisation as a System Engineer for the Aperture Arrays and, since 2017, she has been the Telescope Engineer responsible for the design of the overall SKA low-frequency radio telescope (SKA-Low). Her scientific interests include radio astronomy, radio telescopes, aperture arrays, antenna arrays synthesis both in frequency and time domain, and antenna design and characterization. She is the author of several papers published in international scientific journals and proceedings of international conferences. She is also co-inventor of three patent applications.

VITTORIO GIUSEPPE LOI was born in Lanusei, Italy, in 1989. He received the degree in mechanical engineering from the University of Cagliari, in 2014. After the degree, he worked as a Designer of anodizing plants and packaging machines in Gazzani Engineering srl, Mantova. Since 2017, he has been working as a Designer in Sirio Antenne srl. With Sirio Antenne, he is working on the Square Kilometre Array project (SKA), in particular on SKA-low antenna mechanical design.

ANDREA MATTANA was born in Rome, Italy, in 1980. He received the bachelor's degree in computer engineering for digital control of automation systems at the Roma Tre University in 2008. He gained ten years of experience at the Physics Institute of Interplanetary Space (IFSI-Roma), the National Institute for Astrophysics (INAF) since 2000 becoming Experiment Manager of an Italian payload, the Planetary Fourier Spectrometer (PFS) aboard of the ESA/MarsExpress and ESA/VenusExpress spacecraft missions. Then, in 2010 he moved to Bologna to join the Radioastronomy Institute (INAF/IRA) as a Digital Backend Developer for ESA Space Surveillance and Tracking (SST) and SKA-Low Aperture Array Systems where is also involved in the assembly, integration, and verification activities carried out in Australia.

FABIO PAONESSA (Member, IEEE) was born in Turin, Italy, in 1985. He received the B.S. and the M.S. degrees in biomedical engineering and the Ph.D. degree in electronics engineering from the Polytechnic of Turin, in 2008, 2010, and 2017, respectively. From 2011 to 2012, he was a Research Fellow with the Department of Electronics, Polytechnic of Turin. His activities concerned the design of electronic systems for sonodynamic therapy by means of high-intensity focused ultrasounds emitted by piezoelectric transducers. In 2013, he joined the Applied Electromagnetics Group, Institute of Electronics, Computers and Telecommunication Engineering (IEIIT), Italian National Research Council (CNR), where he is currently a Researcher. His research activities include the scientific applications of the unmanned aerial vehicles for the characterization of antenna arrays and radar systems and wireless sensor networks related applications.

SIMONE RUSTICELLI received the B.Sc. degree in telecommunications engineering from the Engineering School, University of Bologna, in 2012. His thesis was about the measurement and characterization of devices using radio-frequency over fiber (RFoF) technique for radioastronomic applications with Prof. G. Tartarini. He received a two-year scholarship from the Engineering School of Bologna during 2013–2015, studying the possibility of decreasing costs using vertical cavity surface emitting lasers for radioastronomical applications and analyzing gain fluctuation problems in analog single-mode fiber systems. He received a scholarship from the National Institute of Astrophysics of Bologna during 2015–2018. He is currently a Non-Permanent Staff in contract at the National Institute of Astrophysics, Institute of Radio Astronomy, where he is involved in developing and testing LNA and RFoF-based receivers for the low-frequency aperture array, as a part of the square kilometer array; furthermore, the possibility to use high-power lasers to feed remote antennas frontend.

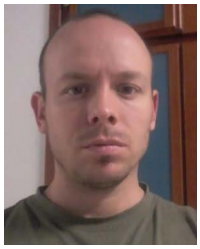

MARCO SCHIAFFINO was born in Castel San Pietro Terme, Italy, in 1982. He received the bachelor's degree in mechanical engineering from the University of Bologna in 2005. After that, he joined the Institute of Radio Astronomy, National Institute for Astrophysics, Bologna, as a Mechanic Technician. He has been responsible for the mechanical upgrade of the Northern Cross Radiotelescope, located in Medicina (BO), and has been involved in several international projects, such as Square Kilometre Array (SKA1-Low) and ESA Space Surveillance and Tracking (SST) where his contribution is mainly focused in the optimization of the antenna designs from a mechanical point of view with particular regards to the integration and housing of RF and optical devices.